Applied Catalysis B: Environmental 237 (2018) 708–720

Contents lists available at ScienceDirect

Applied Catalysis B: Environmental

journal homepage: www.elsevier.com/locate/apcatb

Highly active P-doped sulfided NiMo/alumina HDS catalysts from Mo-blue by using saccharose as reducing agents precursor

José Escobar[a,*], María C. Barrera[b], Ana W. Gutiérrez[a], María A. Cortés-Jacome[a], Carlos Angeles-Chávez[a], José A. Toledo[a], Dora A. Solís-Casados[c]

[a] Instituto Mexicano del Petróleo, Eje Central Lázaro Cárdenas 152, San Bartolo Atepehuacan, G.A. Madero, Cd. de México, 07730, Mexico
[b] Facultad de Ciencias Químicas-Centro de Investigación en Recursos Energéticos y Sustentables, Universidad Veracruzana, Campus Coatzacoalcos, Av. Universidad km. 7.5, Col. Santa Isabel, Coatzacoalcos, Veracruz, 96538, Mexico
[c] Universidad Autónoma del Estado de México, Centro Conjunto de Investigación en Química Sustentable, Km. 14.5 Carretera Toluca-Atlacomulco, Toluca, Estado de México, 50200, Mexico

ARTICLE INFO

Keywords:
Saccharose
Molybdenum-blue
Hydrodesulfurization
$NiMo/Al_2O_3$catalyst

ABSTRACT

Saccharose (SA) was used as organic additive in simultaneously impregnated P-doped $NiMo/Al_2O_3$ hydrodesulfurization (HDS) catalysts (Mo, Ni and P at 12, 3, and 1.6 wt%, respectively). One-pot impregnating solutions were prepared by MoO_3 digestion (~353 K) in diluted aqueous H_3PO_4, followed by $2NiCO_3{\cdot}3Ni(OH)_2{\cdot}4H_2O$ addition. Saccharose (SA, SA/Ni = 0.5, 1–3) was dissolved in originally emerald-green impregnating solutions which changed to cobalt blue by room-temperature aging (2–4 days, depending on SA concentration) due to Mo-blue formation by partial molybdenum species reduction. After sulfiding of samples impregnated with SA shorter MoS_2 slabs of enhanced stacking were observed (by HR-TEM). Ni and Mo dispersion and nickel sulfidability (as determined by XPS) increased with the amount of organic modifier. Enhanced hydrodesulfurization activity in dibenzothiophene HDS was registered for catalyst obtained from Mo-blue precursor as to that of corresponding materials obtained from conventional emerald-green NiMoP impregnating solutions (with or without SA). However, in solids at high saccharose content (SA/Ni = 3) enhanced "NiMoS" phase amount was not reflected in improved activity. Probably, excessive amount of carbonaceous deposits from SA residua decomposition during catalyst activation provoked partially plugged porous network (as determined by N_2 physisorption) in sulfided formulations. That fact seemed to limit accessibility of reactant molecules to surface active sites. Mo-blue precursor obtained through monosaccharides partial reduction seemed to play decisive role in obtaining HDS catalysts of improved properties. Saccharose results a highly soluble, cheap and non-toxic environmentally-friendly additive to produce catalysts of enhanced HDS activity.

1. Introduction

The use of various types of organic additives during hydrodesulfurization (HDS) catalysts preparation has resulted in materials of enhanced S removal activity. For instance, different beneficial effects have been related to chelators addition those mainly being attributed to their strong chemical interaction with the promoters (Ni and Co) [1]. It is well-accepted [1,2] that those complexing organic compounds could enhance molybdenum-promoter interaction during catalyst sulfiding that resulting in materials of increased hydrodesulfurizating activity. Recently, Hensen et al. [2] reported that organic chelators mainly enhance the HDS activity of promoted catalysts more than those of Mo-based unpromoted ones confirming that their main role is improving Co-Mo interaction. Chelation allows promoter sulfidation to temperatures high enough to permit efficient integration of sulfidic Co or Ni species to then already formed MoS_2 (or WS_2), thus optimizing promoted phases ("NiMo(W)S" or "CoMo(W)S") formation. However, for $CoMo/Al_2O_3$ catalysts prepared with nitrilo triacetic acid, Maugé et al. [1] found that in addition to enhanced MoS_2 promotion using that chelator could modify active sites nature. Probably, highly active Type II sites characterized by weakened interaction with the alumina support were formed in that case.

Regarding non-chelating ligands as HDS catalysts additive so far no general agreement about the origin of their beneficial influence has been reached. It appears that enhanced HDS activity could be originated by a number of factors [3–9]. For instance, for P-doped $CoMo/Al_2O_3$ formulations impregnated in glycols presence it has been proposed that the interaction of the organic additive with both basic OH

* Corresponding author.
E-mail address: jeaguila@imp.mx (J. Escobar).

https://doi.org/10.1016/j.apcatb.2018.06.034
Received 16 February 2018; Received in revised form 21 May 2018; Accepted 11 June 2018
Available online 20 June 2018
0926-3373/

groups and coordinatively unsaturated Al^{3+} sites on the alumina surface could partially prevent Co diphosphopentamolybdate (Strandberg heteropolyanions [10]) complexes decomposition during their deposition on the carrier [4]. Thus, close proximity of Co and Mo in those complexes could result in formation of increased amount of the so-called "CoMoS phase" during sulfiding. Others [7] found optimized promoter integration to MoS_2 phase in catalysts prepared in presence of glycols (di-ethyleneglycolbutylether). They observed that Mo and Co sulfidation took place at temperatures up to 473 K, this fact probably contributing to better integration of cobalt promoter to edge sites of molybdenum sulfide particles. Our group reported [3] on the beneficial influence of ethylene glycol added to solutions where the organic additive was simultaneously impregnated with Ni, Mo and P over an alumina support. Again, enhanced formation of promoted "NiMoS" phase appeared to be at the origin of enhanced activity in both model compound (dibenzothiophene) and real feedstock (straigth-run gas oil) hydrodesulfurization. Considering that reported in the pertinent literature, it seems that the positive influence of those organic species on the HDS activity of corresponding catalysts could be related to several independent phenomena. For instance, when comparing the effects of chelating and non-chelating agents on the properties of CoPMo/alumina sulfided catalysts Nikhulsin et al. [11] found that glycols better prevented the decomposition of impregnated 12-molybdophosphoric heteropolyacid $H_3PMo_{12}O_{40}$, as compared to a chelating agent (citric acid). They also observed that active sites turnover frequency (TOF) increased with the (Co/Mo) edge promotion degree in materials prepared with either chelators and no-chelator species or with a mixturte of both modifiers.

Other [12] have used polydopamine biopolymer to coat alumina support where molybdenum was impregnated. The presence of the organic layer was reflected in higher number of Mo adsorption sites as to those over similar material impregnated on bare alumina carrier. The corresponding CoMo-supported catalysts had improved performance for hydrotreating reactions including aromatics saturation, hydrodenitrogenation and gasoil HDS. In that case, better accessibility of reacting molecules and weakened support-impregnated phases interaction due to carbon adlayer were both invoked to explain enhanced catalytic activity in aforementioned reactions.

Saccharose (SA) has been used in the past in developing Co-based Fischer-Tropsch catalysts with alumina as carrier [13]. Using that organic additive resulted in highly dispersed supported phase in reduced catalysts obtained from Co nitrate (Co/SA = 10). It is worth mentioning that in this case saccharose was added during impregnation being then removed during calcining at various temperatures (373–673 K). Thus, no carbonaceous residua were observed, the main effect of the additive being exerted during impregnation step.

Saccharose has also been applied as precursor intended to form carbonaceous materials that could be utilized as catalyst carrier. In this line, composite supports prepared from carbothermal reduction of carbonaceous silicon xerogel obtained by sol-gel by using tetraethoxysilane and saccharose [14] proved to be effective Ru catalysts supports, regarding materials applied in ammonia synthesis.

Regarding saccharose-alumina interaction, some studies have shown that saccharide adsorption follows a typical Langmuirian (S-type) adsorption isotherm, occurring via metal-saccharide interaction and also through electrostatic interactions between surface aluminol groups on alumina and sugar hydroxyls [15]. The exothermic adsorption ($\Delta H^\circ = -9.68\ kcal\ mol^{-1}$) had negative free energy change ($\Delta G^\circ = -6.47\ kcal\ mol^{-1}$) pointing out to its spontaneous nature. Saccharose could be highly dispersed on γ-Al_2O_3 surface at moderate concentrations crystalline sugar being just observed in higly loaded samples ($\sim 0.35\ g_{sugar}\ g_{alumina}^{-1}$) [16]. The partially negatively charged oxygen atoms of hydroxyls in saccharose could establish hydrogen bonding with AlOH groups on alumina surface [15]. Also, interaction of those organic moieties bearing partial negative charge with surface Lewis sites on alumina (Al^{3+} CUS, coordinatively unsaturated sites) could not be discarded.

In previous report [9] we found increased HDS activity (~17% DBT HDS) in alumina-supported NiMo-based catalysts simultaneously impregnated with saccharose by using freshly prepared emerald-green solutions. On the other hand, in the present communication we used corresponding aged cobalt-blue colored impregnating solutions finding much better sulfided catalyst performance. SA was simultaneously one-pot impregnated with Ni, Mo and P components as that easily scalable (for applications at commercial level production) methodology provided HDS catalysts of enhanced activity [9].

Materials were studied by using several textural, structural and surface characterization techniques. Corresponding sulfided catalysts were tested in dibenzotiophene HDS at conditions close to those used in commercial-scale hydroprocessing units aimed to ultra-low-sulfur diesel (ULSD) production.

2. Experimental

2.1. Catalysts synthesis

Commercial powdered boehmite (Versal 200 from Euro Support) was calcined at 773 K (5 h) to obtain high surface area alumina (see Table 1). Pore-filling simultaneous impregnation was carried out over previously dried powder support (393 K, 2 h) with an acidic solution (pH ~2.5) prepared from digestion (at ~353 K, in water and under vigorous stirring, 4 h) of MoO_3 99.5 wt % (PQM) in presence of H_3PO_4, 85.3 wt% (Tecsiquim). H_2O in excess (typically 250 ml of starting solution to impregnate 5 g of alumina carrier) was used to accelerate dissolution and digestion of molybdenum salt. A yellow transparent solution was obtained after approximately 2 h hydrolysis. $2NiCO_3{\cdot}3Ni(OH)_2{\cdot}4H_2O$ (Sigma-Aldrich) was added, processing temperature being maintained for 2 h. Ni concentration corresponded to Ni/(Ni + Mo) = 0.29 molar ratio whereas $P_2O_5/(NiO + MoO_3) = 0.2$ mass ratio was fulfilled [17]. A transparent emerald- green solution was thus finally obtained. The solution volume was then reduced by evaporation until reaching the suitable one for pore-filling impregnation of the given mass of support. The described one-pot impregnation method was chosen as it constitutes a readily scalable methodology during catalyst preparation at commercial scale. It includes cheap industrial precursors easily attainable for commercial catalyst manufacturing. Although not commonly used at laboratory scale preparations [18,19], Ni hydroxycarbonate (soluble in acidic medium) was preferred as nickel source as usage of corresponding nitrate (highly soluble in water) must be avoided due to its explosive properties. Nominal Mo, Ni and P loadings corresponded to 12, 3 and 1.6 wt%, respectively. Phosphorus content closely corresponded to concentration used in preparation of highly active HDS catalysts (Mo/P ~2.5) [20]. Saccharose (SA, J.T. Baker) at SA/Ni molar ratio of 0.5, 1, 2 and 3 was dissolved into the impregnating solutions at room temperature stirring being maintained by 1 h. No appreciable changes neither in pH nor in coloring (emerald-green) was observed after that period of time. However, after room temperature aging the original green coloring of impregnating solutions containing NiMoP-SA changed to cobalt blue. The period of time required to

Table 1
Textural properties (as determined by N_2 physisorption at 75 K) of alumina and SA-modified NiMo/Al_2O_3 sulfided catalysts at different organic additive concentration.

Material	S_{BET} (m^2g^{-1})	S_{BJHa} (m^2g^{-1})	S_{BJHd} (m^2g^{-1})	V_p ($cm^3\ g^{-1}$)	D_p[a] (10^{-9} m)
Al_2O_3	307	375	488	0.90	11.7
SA(0)	224	215	291	0.64	11.4
SA(1)	260	256	354	0.71	10.9
SA(3)	244	231	354	0.59	9.7

[a] From $4\times V_p\ S_{BET}^{-1}$.

observe the blue coloring was function of SA concentration being shortened in solutions of enhanced SA content [21]. For instance, for the solution of the highest organic modifier concentration (SA/Ni = 3) the coloring change took place after 48 h whereas for the one at SA/Ni = 1 blue coloring was registered after about 96 h. No significant effect on pH of pristine impregnating solutions (pH = 2.2) was observed neither after SA addition (non-aged green solution, pH = 2.5) nor after coloring change to blue (pH = 3.4). Alumina support was impregnated by pore-filling with the cobalt-blue solutions at various SA concentrations right after the coloring change from green to blue was observed. Also, a reference matterial was prepared by depositing the SA-modified NiMoP (at SA/Ni) green-colored not aged impregnating solution over corresponding Al_2O_3 carrier. After impregnation, materials were aged overnight at room temperature allowing intradiffusion of impregnated species through the support porous network. Materials were then dried at 393 K (2 h). Calcining was avoided to preserve organic additive integrity. Samples were identified by using the SA(x) key where "x" represented the SA/Ni ratio. Also, when pertinent, subscript "$_g$" (representing "green") was added to previously mentioned keys to differentiate materials impregnated with NiMoP-SA as-made green solutions. A reference material with no organic additive, sample SA(0), was also synthesized. This solid was just dried at 393 K (2 h) before sulfiding.

2.2. Materials characterization

Chemical state of Ni and Mo species present in impregnating solutions was studied through UV–vis spectroscopy by using a Cary 100 instrument (absorbance mode) in the 200–1000 nm wavelength range. Textural properties of support and sulfided catalysts were determined by N_2 physisorption (at 75 K, nitrogen saturation temperature at Mexico City barometric pressure) in a Micromeritics ASAP 2000 apparatus after ultra-high vacuum degassing at 423 K for 6 h. Surface area and pore size distribution of studied materials were determined by BET and BJH (N_2 adsorption and desorption branch data) methods, respectively. Thermal analyses of dried samples were carried out in the room temperature to 1250 K range with a Netzch Thermische Analize STA 409 EP apparatus under static air atmosphere.

Raman spectra of various impregnated samples were obtained using a Jobin Yvon Horiba (T64000) spectrometer, equipped with a CCD camera detector. As excitation source the 514.5 nm line of a Spectra Physics 2018 Argon/Krypton ion laser system was focused through an Olympus BX41 microscope equipped with a 100× magnification objective. Laser power never exceeded 5 mW to avoid damaging the studied samples. Other groups [22,23] have used similar Laser power values during characterization of hydrotreating formulations.

UV-vis diffuse reflectance spectroscopy (DRS) of impregnated samples were carried out on a Perkin Elmer Lambda 35 spectrophotometer equipped with integration sphere. Spectra were taken in the wavelength range from 200 to 1100 nm. Spectralon signal was subtracted as baseline.

Supported sulfidic catalysts were obtained by submitting approximately 0.3 g of ground impregnated precursors (U.S. mesh size 80–100, circa 165 μm average particle diameter) to treatment at 673 K (heating rate 6 K min^{-1}) under H_2/H_2S (Praxair) at 50 ml min^{-1}/6 ml min^{-1} ratio during 2 h. Sulfided catalyst were characterized by electron microscopy and X-ray photoelectron spectroscopy (XPS). High-resolution transmission electron microscopy TEM was performed in a JEM-2200FS at accelerating voltage of 200 kV. The apparatus was equipped with a Schottky-type field emission gun and an ultra-high resolution (UHR) configuration (Cs = 0.5 mm; Cc = 1.1 mm; point to point resolution, 0.19 nm) and in-column energy filter omega-type. Sulfided solids to be analyzed were ground, suspended in isopropanol at room temperature and dispersed with ultrasonic agitation. Then, some drops of obtained suspensions were deposited on a 3 mm diameter lacey carbon copper grid. GATAN™ software was used during statistical determination of slab length and stacking degree in MoS_2 supported particles. Average length and stacking number of MoS_2 slabs ($L_{avg.}$ and $N_{avg.}$, respectively) were statistically estimated through measurements carried out in ~300 $_{MoS2}$ slabs per sample through the following equations:

$$L_{avg.} = \frac{\sum_{i=1\ldots t} n_i L_i}{\sum_{i=1\ldots t} n_i} \quad (1)$$

$$N_{avg.} = \frac{\sum_{i=1\ldots t} n_i N_i}{\sum_{i=1\ldots t} n_i} \quad (2)$$

where n_i is the number of slabs in a given range of length or stacking (L and N, respectively) and t is the total number of analyzed MoS_2 slabs.

Dispersion of molybdenum atoms in MoS_2 crystals was determined by geometrical model from Kasztelan et al. [24]. Thus,

$$D_{Mo} = \frac{Mo_e + Mo_c}{Mo_t} = \frac{\sum_{i=1\ldots t} 6n_i - 6}{\sum_{i=1\ldots t} 3n_i^2 - 3n_i - 1} \quad (3)$$

where D_{Mo} is MoS_2 dispersion, Mo_e, Mo_c and Mo_t are molybdenum atoms on the edges, corners and total ones (as determined by slabs size); n_i is the number of atoms along one side of a molybdenum sulfide slab as determined from its length, $L = 0.316 \times (2n_i\text{-}1)$, in nm, and t is the total number of slabs analyzed from HR-TEM corresponding micrographs during the statistical counting.

XPS spectra were obtained in a THERMO-VG SCALAB 250 spectrometer equipped with $Al_{K\alpha 1}$ X-ray source (1486.6 eV) and a hemispherical analyzer. Experimental peaks were decomposed into components using mixed Gaussian-Lorentzian functions and a non-linear squares fitting algorithm. Shirley background subtraction was applied. Binding energies were reproducible to within ± 0.2 eV and the C 1s peak (from adventitious carbon) at 284.6 eV was used as a reference. Surface elemental composition was determined by fitting and integrating the Ni (2p), Mo (3d), S (2 s), P (2p) and Al (2p) signals intensity and converting these values to atomic ratios by using theoretical sensitivity factors provided by the manufacturer of the XPS apparatus. Sulfided catalysts were kept under inert atmosphere to avoid samples oxidation by using a glove box and a special box vessel to introduce the samples into the spectrometer analysis chamber.

2.3. HDS reaction test

Impregnated precursors were sulfided at 673 K (heating rate 6 K min^{-1}) under H_2/H_2S (Praxair) at 50/6 (ml min^{-1})/(ml min^{-1}) during 2 h. HDS activity of the obtained sulfided catalysts was studied in a triphasic slurry batch reactor (Parr 4575). The reaction mixture was prepared by dissolving ~0.3 g of dibenzothiophene (model of organo-S species in middle-distillates) in 100 cm^3 of n-hexadecane (representing hydrocarbon matrix in straight-run gasoil) (98 mass % and 99+ mass %, respectively; both from Aldrich) and adding ~0.2 g of sieved catalyst (80–100 U.S. mesh, ~0.165 mm average particle diameter). Operating conditions, carefully chosen to avoid external diffusion limitations [9], were P = 7.1 MPa, T = 593 K and 1000 RPM (~105 rad s^{-1}, mixing speed). Samples were taken periodically and analyzed by gas chromatography (Agilent 6890 N with flame ionization detector and Econo-Cap-5 capillary column length: 30 m, 0.53 mm diameter and film thickness of 1.2 μm, from Alltech). HDS kinetic constants were calculated assuming pseudo-first order model referred to DBT concentration and zero order with respect to excess H_2:

$$k = \frac{-\ln(1-x)}{t_r} \quad (4)$$

where x is conversion and t_r refers to reaction time. k values for various catalysts were normalized by considering reaction volume and mass of catalyst used (k^1 in m^3 $kg_{cat.}{}^{-1}s^{-1}$)). According to constant slope of $-\ln(1\text{-}x)$ versus reaction time plots in the dibenzothiophene HDS over various tested materials tested (see, for instance, Fig. S1) significant

deactivation along the duration of our catalytic tests could be ruled out. Thus, in our case calculation of k (pseudo first order kinetic constant) we considered all the experimental points obtained during duration of our reaction tests. On the other hand, declining slope at progressively longer reaction times in corresponding -ln(1-x) versus reaction time plots in the case of supported Pd-Pt catalysts tested in the HDS of sterically-hindered dibenzothiophenic species in batch reactor have been related to catalysts deactivation [25].

HDS activity of various materials was also compared on per active sites basis by affecting intrinsic activity (on per Mo mass basis) taking into account corresponding Mo^{4+} fraction and dispersion (as determined by XPS analysis and from Eq. (3), respectively) over different prepared catalysts [26].

3. Results and discussion

3.1. Visible spectra characterization of impregnating solutions

To discern the chemical phenomena behind color changes of impregnating NiMoP-SA solutions after aging we studied corresponding liquid samples by visible region spectroscopy. To determine if Ni promoter chelation took place in the impregnating solutions Ni hydroxycarbonate and H_3PO_4 were dissolved at concentration equivalent to that used during catalysts preparation Due to its strong absorbance the sample was diluted with water (5:1). Characteristic green-emerald coloring imparted by hexa-aquonickel cations ($Ni[(H_2O)_6]^{2+}$) was observed, the corresponding visible spectra showing absorptions at 657 and 723 nm due to octahedral $Ni^{2+}_{(Oh)}$ [27], Fig. S2. After organic additive addition (at SA/Ni = 1) no significant changes were evidenced even after several days room temperature aging (maxima at 663 and 724 nm, Fig. S3) meaning that water molecules in $Ni[(H_2O)_6]^{2+}$ were not substituted by stronger (in spectroscopic series [28]) organic ligands (carboxylates, for instance). Nickel complexation under those conditions could be then ruled out. Although preparation of chelated iron cations with fructose has been reported [29,30] nickel complexation appeared improbable as disaccharides lack this ability [30].

In the opposite and as already mentioned, when sucrose was added to impregnating solutions containing NiMoP the original green coloring shifted to cobalt blue after room temperature aging for some days, depending on SA concentration. Visible region spectra in Fig. 1 show evolution of spectra corresponding to impregnating solutions through different preparation stages. Due to different absorbance of studied samples dilutions (with water) were required. Dilution factors used are shown in Fig. 1 caption. Pristine NiMoP solution and the as made SA-modified one ($SA(1)_g$) showed characteristic $Ni^{2+}_{(Oh)}$ [27] absorptions (Fig. 1(a) and (b), respectively) whereas aged deep blue solution registered peaks related to molybdenum-blue complex (Fig. 1(c)). Similar signals with peak maximum at 865 nm and shoulder at 700 nm were considered by Shukor et al. [31] as unique fingerprint characterizing Mo-blue compounds from phosphomolybdates reduction using various carbohydrates as electron donors. Also, Yoshimura et al. [32] obtained Mo-blue species (visible spectra maxima at 890 and 710 nm) from phosphomolybdates reduction by ascorbic acid pointing out that those P-containing compounds are important intermediates in partial Mo reduction.

Cáceres et al. [33] identified Mo-blue species after X-ray irradiation in XPS equipment chamber that provoked elimination of lattice oxygen from MoO_6 octahedra followed by rearrangement of produced defective structures. Also, Louis and Che [34] reported air oxidation of physisorbed Mo_5Cl_{10} on silica into molybdenum-blues. In this case, however those species were eliminated after washing with ammonia solution due to their very weak interaction with the support. To the best of our knowledge, just a few papers reports on using Mo-blue as heterogeneous catalyst or catalyst precursor. For instance, Hutchings et al. [35] reported utilizing Mo-blue nanorings with Mo^{5+}/Mo^{6+} ratio = 1/4 founding excellent activity and stability in the partial oxidation of cyclohexane to cyclohexanol and cyclohexanone.

Saccharose has been added to solutions containing disolved MoO_3 which were maintained at 353 K until color changed from orange to blue. According to the authors, that indicated Mo^{6+} reduction to colloidal molybdenum-sucrose complex [36]. The dark blue grains obtained after drying were carburized the final material presenting promising properties in the methane dry reforming.

Regarding hydrotreating catalysts the preparation of highly active Mo-blue based sulfided catalysts applied in thiophene HDS and pyridine hydrodenitrogenation was previously reported [37]. However and in spite of very promising results obtained no further investigations by using promoted (by Co or Ni) catalysts were further published. In mentioned paper hydrazine sulfate was used as reductant, the product showing visible spectra maximum at 775 nm. The structure was considered as that of $[Mo_6O_{18}]^{-2}$ anion. Srinivasan et al. [38] also used hydrazine-hydrochloric acid solution although in this case Mo-blue coloring was just used as visible indicator of molybdenum diffusion through alumina pellets. However, susbstitution of hydrazine sulfate as reducing agent by citric acid for Mo-blue formation has been proposed [39] due to its extreme toxicity and carcinogenicity that makes impractical its utilization. Interestingly, Srinivasan et al. [38] failed in obtaining Mo-blue by using sucrose as reducing agent eve after heating at 373 K heating. Very probably at the high pH conditions of ammonium paramolybdate solutions they used the non-reducing disaccharide could not be properly hydrolyzed to reducing fructose and glucose. That reaction easily takes place in acidic medium [41]. It is worth mentioning that Mo-blue generically refers to partially reduced molybdenum species with average oxidation number of Mo is between 5.5 and 6 and which exact nature depends on formation conditions (type of reducig agent, pH of solution, etc.) [40]. Thus, changing the synthesis conditions could result in various Mo-blue species which could have very different characteristics as HDS catalysts precursor.

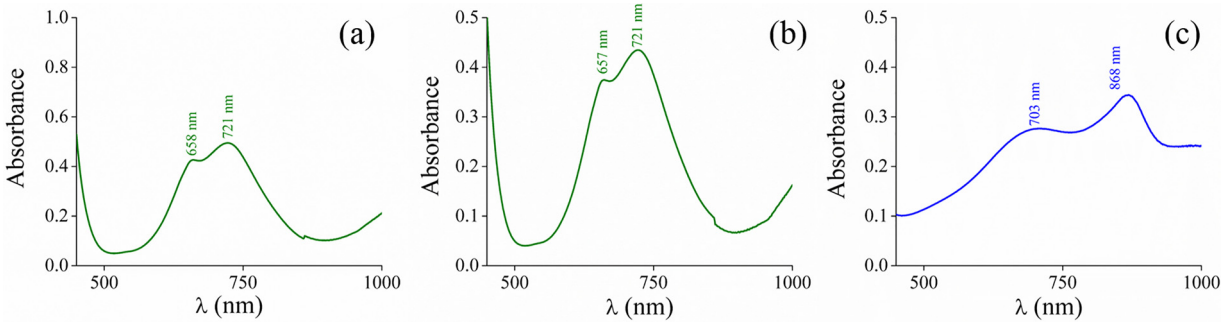

Fig. 1. (a) Visible region spectrum of Ni hydroxycarbonate + H_3PO_4 + MoO_3 + saccharose solutions originally at concentrations similar to those used during catalysts preparation. (a): As made NiMoP solution, diluted with water 2.5:1; (b): SA-modified, non-aged ($SA(1)_g$) impregnating solution, diluted with water 2.5:1; SA-modified impregnating solution aged until Mo-blue formation, diluted with water 500:1. (For interpretation of the references to colour in the figure text, the reader is referred to the web version of this article.)

In order to be able to act as reductant a given sugar requires the presence of hemiacetal moieties, i.e., a carbon linked to both one OH− and one OR− group. In that way, the cyclic sugar could be in equilibrium with an open-chain linear isomeric form containing an aldehyde group that could be oxidized to corresponding carboxylic acid, with the consequent reduction of involved oxidizing agent (Mo^{6+} species in our case). On the other hand, saccharose have glycosidic bonds between its anomeric carbons (acetal moieties) joining glucose and fructose rings and thus could not be converted to an open-chain isomer forming an aldehyde. However, saccharose in aqueous solution could be easily hydrolyzed into monosaccharides components under highly acidic conditions (pH ~ 2) [41] (see Scheme S1), as in the case of our NiMoP one-pot impregnating solutions (see Section 2.1 Catalysts Synthesis). Glycosidic bonds linking glucose and fructose rings could be then readily hydrolyzed converting saccharose into those monosaccharides very well-known for their reducing properties. In our case, as the open-chain linear isomeric form of monosaccharides (containing an aldehyde group to be oxidized) could disappear by reacting with Mo^{6+} species their consumption could progressively displace thermodynamic equilibrium to its fomation providing enhanced amounts of reducing agents. Through their oxidation glucose and fructose could be able to originate corresponding carboxylic acids (saccharic acid from the former, glycolic and trihydroxy-butyric ones from the latter) which could then carry out cations chelation. However, in order that phenomenon to take place pH during impregnation over alumina surface must be high enough to allow weak organic acids deprotonation to permit then Ni-complexation. Advantageously, those oxidated derivatives could probably complexate nickel promoter in our impregnating solutions.

The saccharide and its oxidized derivatives could also form carbonaceous deposits able to weaken the supported phases-carrier interaction [9]. In fact, in previous investigations we found that in SA-modified alumina-supported sulfided NiMoP formulations obtained from non-aged green solutions (where no reduced Mo-blue species existed) carbonaceous residua from the disaccharide decomposition during catalyst activation by sulfiding resulted in enhanced HDS activity in dibenzothiophene conversion. In that case, alumina surface passivation weakened carrier-deposited species interaction that being reflected in ~17% enhanced HDS activity, as to that of non-modified otherwise similar NiMoP/alumina conventional catalyst. All those mentioned effects could positively influence the properties of corresponding HDS catalysts. Although Mo-blue could be obtained through the use of other reducing agents we emphasize that this work was focused in using an additive which characteristics could allow its application in commercial level catalysts manufacturing. The use of a readily scalable preparation protocol including no additional preparation steps in our case was of crucial importance. It is worth mentioning that Mo-blue obtention in SA-modified NiMoP impregnating solutions could be accelerated by heating at 353 K where the partially reduced molybdenum species could be almost instantaneously formed. Thus, SA results a very convenient, cheap, environmentally friendly additive. Finally, the low pH of impregnating solution containing nickel and phosphopentamolybdates species provides the ideal environment for SA acid hydrolysis for in situ formation of monosaccharides actually acting as reducing agents. Again, by avoiding the direct addition of glucose, fructose or a mixture of them the proposed preparation process is simplified by utilizing a readily available disaccharide significantly cheaper than its corresponding hydrolysis products.

In the following, characterization of Mo-blue based Ni promoted catalysts was endeavoured to try to get insigth into the effect of using that precursor on HDS properties of corresponding sulfided catalysts.

3.2. Textural characterization of materials

N_2 physisorption isotherms (Fig. S4) of alumina and corresponding sulfided catalyst SA(0) were intermediate between types II and IV according to IUPAC classification [42] suggesting mesoporosity and perhaps some macroporosity. In SA(0) adsorbed N_2 volume decrease, as to that of alumina support, was proprotional to the non-porous NiMoP phases loading in sulfided catalyst (~29 wt%) ruling out partial pore-plugging then suggesting well dispersed impregnated phases. Isotherm corresponding to SA(1) (Fig. S4) was similar as to that of the non-modified SA(0). However, in SA(3) N_2 adsorption capacity had clearly diminished probably due to enhanced amount of carbonaceous deposits partially plugging the porous network.

Alumina and SA(0) materials had type H1 hysteresis characterizing solids with porous networks of uniform size and shape [42] where capillary condensation [43] started at $\sim P/P_s = 0.45$. On the other hand, in SA-modified solids the hystheresis shape progressively shifted to H3 type suggesting presence of slit-shaped pores of non-uniform size and/or shape [42] that could be provoked by pore mouth narrowing [44]. In these cases, capillary condensation started at approx. $\sim P/P_s = 0.40$ suggesting smaller pores as to those of SA(0). Then, carbon deposits were suggested, mainly on the SA(3) solid.

Carrier surface area loss in SA(0) was commensurated with deposited NiMoP phases (Table 1) loading supporting the notion of well dispersed sulfidic non-porous phases. Interestingly, SA-modified samples had augmented surface area as to that of non-modified SA(0), pointing out to additional contribution from void spaces in porous carbonaceous deposits. Similar results were reported by Rinaldi et al. [45] in the case of sulfided Co-Mo/B_2O_3/Al_2O_3 catalysts prepared with citric acid. In SA(3) incremental surface area could be counterbalanced by decreased pore volume due to more significant amount of carbonaceous deposits.

To determine which pore size distribution profile (PSD, through Barret-Joyner-Halenda, BJH, methodology) obtained from either adsorption or desorption data branch (Figs. S5 and S6, respectively) better represented the actual one corresponding cumulative surface area values were compared to those obtained through the BET method, Table 1. As values from adsorption branch data (S_{BJHa}) were closer to the BET ones we considered that PSD profiles from those data were the most reliable to describe the actual porous networks.

From Fig. S5, a proportion of the smaller pores existing in alumina support network disappeared after NiMoP phases impregnation. Whereas SA(1) BJH_a PSD was similar in both SA(0) and SA(1), the maximum at ~12 nm in the latter profile decreased by 50% in the SA(3), again pointing out to partial pore-plugging by increased carbonaceous deposits. The SA-modified catalysts PSD profile from desorption data (Fig. S6) had maximum at ~3.2 nm that was much more remarkable in SA(3). We considered that an artifact due to tensile strength effect (TSE) originated by random distribution and interconnectivity of pores [46] that commonly appears by the sudden forced closure of hystheresis at P/P_s between 0.4–0.45 and 0.4–0.5 for SA(1) and SA(3), respectively. If that PSD maximum around 3.8 nm were real it must be evident in profiles obtained from both adsorption and desorption data branches. It is worth mentioning that several investigators have been misled by aforementioned effects attributing corresponding PSD maximum to porosity creation [46]. For instance, a peak between 3–4 nm have been reported for SA-impregnated alumina at content superior to monolayer [47] that being dubiously attributed to carbonaceous deposits from crystalline SA carbonization. Taking into account that our SA-modified catalysts manifested pore network effects the PSD from adsorption branch was deemed more representative of the actual as it was not significantly affected by TSE phenomenon, as already suggested by comparing corresponding S_{BJHa} surface area data (Table 1) with corresponding S_{BET} ones.

3.3. Thermal analysis (TG-DTA) of impregnated solids

Up to 366 K (water boiling temperature in Mexico City) weight losses of around 3.3% were registered in both alumina impregnated with SA and phosphate (at concentrations similar as to those in SA(1) dried formulation, Fig. S7. In the former case, phosphates were added

in concentration similar to that used in impregnating solutions due to the effect of those anions on amount of saccharide adsorbed by the carrier. The electrostatic repulsion between the alumina $AlOH_2^+$ groups of the positively charged support surface under acidic conditions due to its isoelectric point [48] and partially charged hydrogen in $-OH^+$ groups of saccharides could be screened by the added phosphate anions then significantly increasing the amount of adsorbed organic species [15]. Also, interaction between the negatively charged oxygens $-HO^{\delta-}$ and aluminols could be favored. Although carbohydrates are slightly acidic in aqueous solutions [15] under the low pH conditions provided by dissociated H_3PO_4 they could not be deprotonated that precluding its interaction with coordinatively unsatured sites of surface Al^{3+} cations. Organic matter decomposition and combustion were related to additional losses (~23 wt%) up to 773 K, Fig. S7.

Physisorbed species were diminished on SA(1) and SA(3), as to that in the alumina modifed by SA and phosphates probably due to surface coverage by deposited species Weigth losses due to organic matter decomposition and combustion were notably accelerated by Ni and Mo phases acting as combustion catalysts [49]. In SA(1) increased losses related to mentioned phenomena suggested presence of species of weaker interaction with the support. In the 366–773 K weight losses in analyzed dried samples SA(1) and SA(3) were 22 and 35 wt%, respectively. According to saccharose composition about 42% of those weigth losses could be attributed to carbon species (i.e., ~9 and ~15 wt%, respectively). Beyond ~1090 K MoO_3 sublimation [49] was reflected in pronounced weight losses in Mo-containing solids.

Endothermal signals due to melting and decomposition of saccharides were absent in profiles of SA-containing samples of Fig. 2 pointing out to adsorbed species in chemical interaction with the alumina support [47]. The signal at approximately 470 K and the wide exothermal inflexion between ~540–755 K were both related to combustion of species bonded to the carrier. Indeed, this kind of carbonaceous deposits have been related as support-like carbon which participates in the structure of the active phase as an intermediate carrier decreasing their interaction with the alumina support, as proposed by Chianelli et al. [50] from their studies on $CoMo/Al_2O_3$ catalysts modifed by ethylenediamine.

Exothermal peaks at 773 and 1080 K were originated by NiO crystallization and $Ni_2Al_{18}O_{29}$ formation, respectively, due to high-temperature migration and sintering of nickel species. The small endothermal signal at 1230 K in Mo-containing samples could be originated by MoO_3 sublimation [49].

The strong exothermal peak at 514 K in SA(1) profile shifted to 546 K in SA(3) showing significantly enhanced intensity in agreement with its augmented saccharide content. Those inflexions could be related to organic moieties in interaction with deposited phases. It seemed that in SA(3) more stable metal-organic complexes could be formed. In this line the visible region signal around 400 nm previously identified in SA-containing alumina-supported NiMo formulations [9] could be rather attributed to ligand to metal charge transfer (LMCT) complexes saccharide-molybdenum. Indeed, absorptions due to LMCT complexes of thioglycolic acid-molybdenum have been identified in that region [26,51].

3.4. Raman spectroscopy studies of impregnated samples

According to the Mo/P ~2.5 ratio used during our catalyst preparation (~2.5) and the pH of impregnating solutions (~2.5) Strandberg $H_2P_2Mo_5O_{23}^{4-}$ anions constituted by two PO_4 tetrahedrons surrounded by five interconnected octahedral MoO_6 species could be preferentially formed in impregnating solutions obtained from MoO_3 digestion in diluted H_3PO_4 [4,52]. Also, due to their stability $H_xP_2Mo_5O_2^{(6-x)-}$ anions could exist in different protonation states over a wide pH range [52]. Then, those species could be preserved after the slight pH changes observed after SA addition. However, after contacting the γ-Al_2O_3 carrier surface due to increased pH that species start decomposing into phosphate and molybdates [53]. In agreement with that, deposited Mo species in dryed precursor prepared with no SA (inset in Fig. 3) showed Raman absorptions at 225, 359, 913 (shoulder) and 949 cm^{-1} that could be assigned to Anderson-type Al $(OH)_6Mo_6O_{18}^{3-}$ species [4] which formation could involve partial carrier dissolution. The former two signals could be assigned to Mo—O—Mo and O—Mo—O vibrations [54], meanwhile those at higher wavenumbers were related to Mo=O bands. The shoulder at 1085 cm^{-1} suggested deposited polyphosphates originated by phosphomolybdates decomposition [6]. Interestingly, the M=O stretching vibration shifted to 969 cm^{-1} in SA-containing samples strongly suggesting octahedrally-coordinated $Mo_8O_{26}^{4-}$- or $Mo_7O_{24}^{6-}$-like isopolymolybdate species [55]. Similar signals have been associated to hydrated molybdates [56]. In our case, OH´s could be partially provided by organic moieties closely interacting with deposited Mo species. Also, organic moieties could compete with heteropolymolybdates-like species present in solution during impregnation. Some organic moieties could deposit on surface OH groups and Al^{3+} sites. Thus, interaction between diphosphopentamolybdate-like anions and the alumina support could be diminished. Through this mechanism, decomposition of those impregnated species could be prevented at some extent. Once deposited, those species could be precursors of polymolybdates observed in Raman spectra of SA-containing sample (Fig. 3). The shoulder at 985 cm^{-1} in SA-containing materials (more notable in SA(3)) was related to Mo=O symmetric stretch of well-

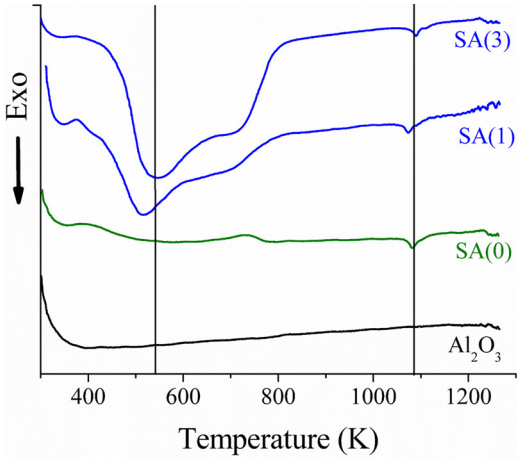

Fig. 2. Differential thermal analysis (under static air atmosphere) of dried samples of Al_2O_3 carrier, SA(0), SA(1) and SA(3) impregnated samples.

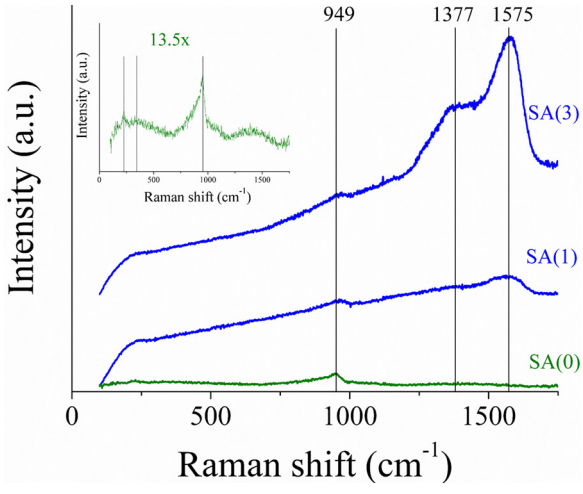

Fig. 3. Raman spectra of SA(0), SA(1) and SA(3) impregnated samples.Inset: Magnified (13.5×) SA(0) spectrum.

defined, three-dimensional molybdate clusters [57] in agreement with Mo-species in lower interaction with the carrier.

Two bands due to deposited carbonaceous species could be clearly identified in Raman spectra of SA-modified materials (Fig. 3). The D band centered around 1377 cm^{-1} and the eco band at 1613 cm^{-1} (D2, shoulder) could be assigned to disordered or poorly structured aromatic moieties whereas the shoulder observed between 1510–1530 cm^{-1} could be attributed to D3 band related to structural defects of poorly-organized aromatic domains [58]. More structured aromatic clusters originated the G band at 1580 cm^{-1}. All mentioned signals were much more intense in SA(3) spectrum indicating increased carbonaceous deposits amount. This fact agreed with the enhanced height/width G band ratio in SA(3) as to that of SA(1) pointing out to larger carbon clusters in the former material. It should be mentioned that some carbonaceous deposits heating and graphitization could occur due to the laser power used during Raman analysis (less than 5 mW) [59]. Expectedly, those deposited carbon residua could play a determining role in the HDS catalytic activity of prepared formulations. That kind of carbonaceous deposits could be partially playing support-like role [50] as suggested by our DTA results (see Section 3.3 Thermal analysis (TG-DTA)) decreasing the deposited phases-alumina carrier interaction. However, if massive, formation of carbon deposits could also affect textural properties of corresponding catalysts as found by N_2 physisorption (see Section 3.2 textural characterization).

Interestingly, it has been proposed that carbonaceous deposits could act as reservoir of molecular H_2 dissociated on MoS_2 phases which could then spillover onto the basal planes of graphite-like species through reaction of atomic H with *p* electrons in the basal plane of those carbon species [60]. Accumulated hydrogen stored in deposited carbon could be then delivered to "CoMoS" sites (or "NiMoS" in our case) during the course of HDS reactions significantly enhancing sulfur removal activity [61].

3.5. Characterization of SA-modified $NiMo/Al_2O_3$ and $CoMo/Al_2O_3$ impregnated solids by UV–vis spectroscopy

Comparison of visible spectra of SA-modified $NiMo/Al_2O_3$ oxidic formulations impregnated with green (as made) and blue solutions (Fig. 4(a) and (b), respectively) evidenced Mo-blue species characterized by maximum at 698 nm [31] in the latter case whereas in the former absorptions due to octahedral Ni^{2+} [27] could be identified. Formation of LMCT saccharide-Mo complex where molybdenum atoms could be partially reduced could be related to absorption at 403 nm [26] in Mo-blue containing sample. Position of bands due to LMCT complexes depends on local symmetry of Mo^{6+} and Mo^{5+} cations originated by their coordination and aggregation state [62].

In order to assess the feasibility of synthesizing Mo-blue precursors also in the case of alumina-supported CoMo catalysts corresponding solutions were prepared by using similar methodology (Co/SA = 1) to that used in the case of Ni-based formulations (see Section 2.1. Catalysts Synthesis). The original wine-colored solution (CoMoP-SA) turned very dark after heating at ~353 K. In this case, for sake of simplicity, heating was applied to accelerate saccharose acid hydrolysis (see Scheme S1) conditions at which Mo-blue formation took just some minutes. After alumina impregnation by pore-filling, the dried material ($SA_{CoMo}(1)$) was analyzed by UV–vis DRS. A calcined sample prepared with no SA ($CoMo/Al_2O_3$) was also studied as reference, Fig. S8. In addition to well-known signal at 250 nm corresponding to tetrahedral molybdenum species the inflexion at 337 nm in $CoMo/Al_2O_3$ was related to octahedral ones [9]. That signal red-shifted to 355 nm in $SA_{CoMo}(1)$ spectra suggesting larger polymolybdates domains [9] in agreement with that found by Raman spectroscopy in Ni-based formulations (see Fig. 3 and Section 3.4). Similarly to the case of SA-modified $NiMo/Al_2O_3$ sample impregnated with blue solution absorption at 403 nm evidenced LMCT saccharide-Mo complex [26]. Signals at 700 and 867 nm related to Mo-blue species [31] were clearly identified. On the other hand, on conventional non-modified $CoMo/Al_2O_3$ in the visible region a triplet with maxima at 540, 590 and 642 nm characterized tetrahedral Co^{2+} species [63]. Enhanced background absorption in visible spectrum range for SA-containing sample was provoked by its dark coloring. Finally, the possibility of easily obtaining supported Mo-blue precursors also in Co-based formulations by using the used synthesis methodology was proven.

3.6. Sulfided catalysts characterization of by high-resolution electron microscopy (HR-TEM)

From corresponding electron micrographs (Figs. 5(a)–(e) and S9) some changes in MoS_2 particles morphology caused in prepared sulfided catalysts by SA addition at various contents were detected (Table 2). It was determined that average stacking degree of MoS_2 fringes of around 0.62 nm interplanar *d*-spacing (S—Mo—S layers in (002) plane) slightly increased whereas slab length diminished in samples prepared by saccharide addition, even at the lowest modifier concentration (SA/Ni = 0.5, SA(0.5)). Average MoS_2 slab length in sulfided SA(0) formulation (Table 2 and Fig. 5(a)) was larger as compared with values commonly reported in the literature for similar catalysts. However, it should be considered that our samples had rather weak interaction with the support as they were not annealed at high temperature (see Section 2.1 Catalyst synthesis). In this line, Duan et al. [64] identified MoS_2 slabs of 5.6 nm average length in $NiMo/\theta\text{-}Al_2O_3$ materials where the low surface hydroxyl concentrations that characterizes the used alumina phase carrier precluded high deposited phases-support interaction. Even lower carrier-deposited phases interaction in SA-modified samples due to support-like carboceous remains could be reflected in more stacked MoS_2 slabs during catalysts sulfiding

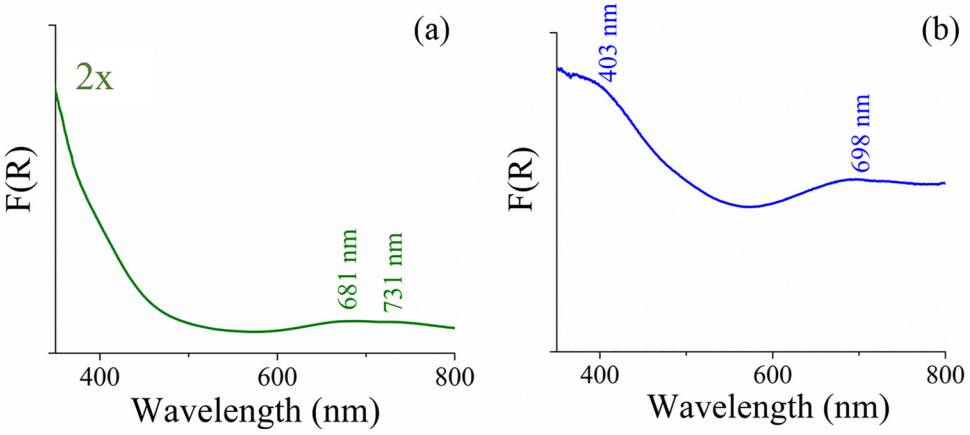

Fig. 4. UV–vis DRS spectra (Schuster-Kubelká-Munk function) of P-modified NiMo/alumina prepared with saccharose (at SA/Ni = 1). (a): Impregnated with green non-aged solution, $SA(1)_g$; (b): Impregnated with Mo-blue containing solution, SA(1). (For interpretation of the references to colour in the figure text, the reader is referred to the web version of this article.)

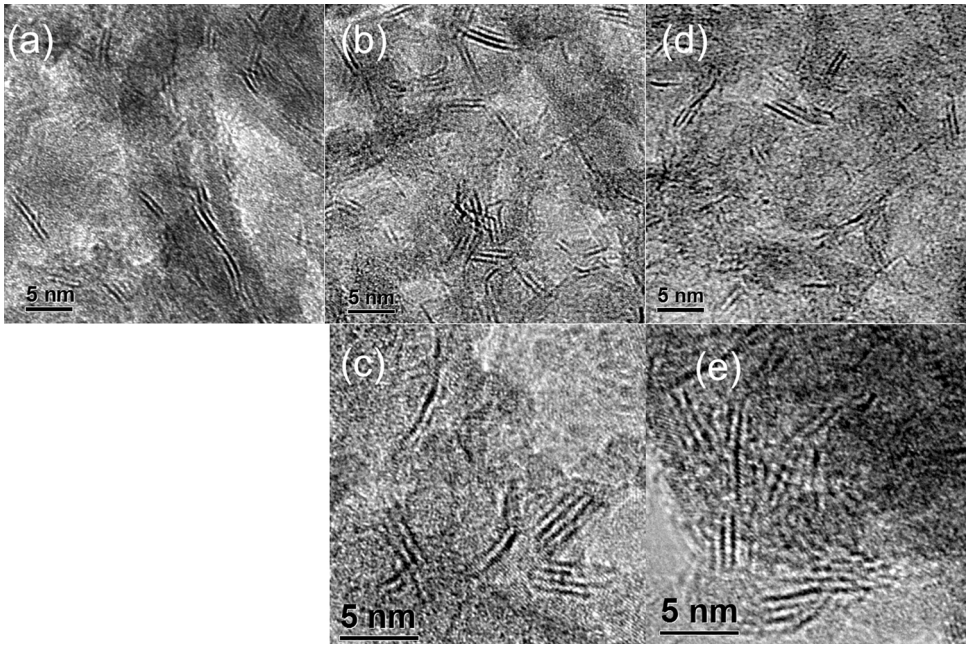

Fig. 5. HR-TEM micrographs of various sulfided catalysts prepared. (a): SA(0); (b) and (c): SA(1); (d) and (e): SA(3).

Table 2
Statistical distribution of stacking and length of MoS_2 slabs over various sulfided catalysts prepared from corresponding HR-TEM micrographs (see Fig. 5 and Fig. S9). Sulfided molybdenum dispersion (D_{Mo}) also included.

Catalyst	Stacking	Slab length (nm)	D_{Mo} [a]
SA(0)	3.4 ± 0.60	6 ± 0.50	0.20
SA(0.5)	3 ± 0.55	4 ± 0.90	0.29
SA(1)	4 ± 0.60	4 ± 1.10	0.29
SA(2)	4 ± 0.70	3.5 ± 1.10	0.33
SA(3)	4 ± 0.65	4 ± 1.00	0.29

[a] Mo^{4+} dispersion calculated from Eq. (3).

(Table 2 and Figs. 5(b)–(e) and S9).

That fact suggested, again, weakened MoS_2-support interaction in samples prepared with SA probably due to deposited carbon residua playing support-like role [50] in agreement with our DTA and Raman spectroscopy results (see Sections 3.3 y 3.4, respectively). As stacking of sulfided Mo particles was not affected by increased amount of carbonaceous deposits over SA(3) as to those over SA(1) preferential deposition of excess organic residua on bare alumina support was suggested. Additionally to the partial Mo^{6+} reduction provoked by formation of LMCT complex and according to D_{Mo} data in Table 2 saccharose could contribute to significantly enhanced alumina-supported molybdenum sulfide particles dispersion. It should be taken into account, however, that information provided by conventional HR-TEM could be limited as it provides insight of imaged "edge-on" sulfided Mo particles contacting the Al_2O_3 support through edge planes (100) and (110) perpendicular to the S-Mo-S layers where slabs appeared as lines. Details about morphology of those crystallites contacting the carrier through the (001) basal plane parallel to S—Mo—S layers could remain then undetected [65]. That could be provoked by invisibility (by HR-TEM) of basal-bonded MoS_2 slabs [65] that could indeed be more abundant in the catalysts of higher Mo-carrier interaction (among our formulations, the one with no organic modifier SA(0)). Note the apparent lower population of MoS_2 slabs in Fig. 5(a), as to those in the rest of micrographs included.

Decreased interaction between alumina carrier and deposited MoS_2 due to "sandwiched" carbonaceous deposits could favor formation of so-called Type II sites [66] characterized by having significantly augmented HDS activity as to that of conventional Type I sites [67].

Carbonaceous residua could also act as spacer hindering sulfided phases sintering thus improving their dispersion. In this line, Yi et al. reported [68] preparation of NiMo-based catalaysts in presence of polyethylene glycol (PEG) by using their solvent-free solid-state method. Based in their results that group claimed that when in suitable amount PEG addition rendered materials of improved sulfidability and active MoS_2 dispersion the latter effect being caused by carbonaceous residua blocking Ni and Mo phases aggregation avoiding then formation of large clusters.

3.7. Characterization of sulfided catalysts by X-ray photoelectron spectroscopy (XPS)

Mo 3d region XPS profiles corresponding to various sulfided $NiMoP/Al_2O_3$ catalysts studied are shown in Fig. 6. Decomposition of registered signals provided the data summarized in Table 3. Mo signals were fitted considering doublets (corresponding to $3d_{5/2}$ and $3d_{3/2}$ contributions) due to Mo^{6+} (MoO_x), Mo^{5+} (MoO_xS_y) and Mo^{4+} (MoS_2) species [69]. Oxidic molybdenum species dispersion (Mo^{6+}/Al, column 4 of Table 3) progressively decreased by saccharide addition in SA(1) and SA(2) suggesting competition between Mo species and organic moieties for adsorptive sites on alumina surface [15]. Also, total molybdenum (oxidic + oxysulfides + sulfides, Mo_T/Al, column 5 of Table 3) dispersion decreased in SA(1) as to that in SA(0) probably by aforementioned effect. Decreased Mo-carrier interaction in SA-modified samples could also contribute to lower molybdenum dispersion in agreement with that found in previous studies [9] by temperature programmed reduction where tetrahedral Mo^{6+} species in high interaction with the alumina support were essentially absent in SA-modified $NiMo/Al_2O_3$ impregnated samples prepared with non-aged as-made green solutions. At high SA concentration, however, it seemed that large amount of deposited carbonaceous residua (see Section 3.4 Raman spectroscopy) could contribute to disperse molybdenum species [70].

Oxysulfides dispersion (Mo^{5+}/Al, column 3 of Table 3) was clearly diminished in SA-containing solids. In those cases, decreased concentration of that species could be probably related to facilitated Mo^{4+} formation from partially reduced entities already extant in Mo-blue

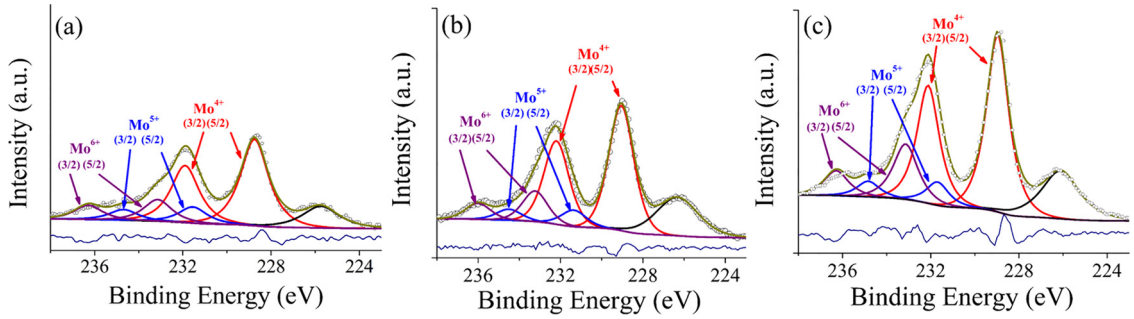

Fig. 6. XPS envelope of Mo 3d region of sulfided P-doped NiMo/Al_2O_3 catalysts prepared with or without saccharose. Peak decomposition to various Mo species considered also shown. (a) SA(0); (b) SA(1); (c) SA(3).

species [40] present in formulations modified by saccharide addition. Sulfided Mo^{4+} species dispersion (column 2 of Table 3) showed different trend as to that found by our HR-TEM studies (column 4 of Table 2) where that parameter augmented in SA-containing samples. That could be provoked by aforementioned invisibility (by HR-TEM) of basal-bonded MoS_2 slabs [65] that could indeed be more abundant in the catalysts of higher Mo-carrier interaction (among our formulations, the one with no organic modifier SA(0)). It should also be taken into account that geometrical model proposed by Kasztelan [24] rather than considering total molybdeum sulfide dispersion emphasizes the proportion of exposed Mo^{4+} atoms located on slab edges and corners, being then potential active HDS reaction sites.

Differently to that observed for sulfided catalysts prepared with ethyleneglycol as modifier [3], Mo sulfidability [71] (column 6 of Table 3) augmented in SA(1) and SA(3), as to the sample prepared with no additive. Again, that could probably due to the presence of intermediate partially reduced Mo^{5+} species already present in solids impregnated with the saccharide (Mo-blue LMCT species) that facilitated molybdenum species sulfidation. In this regard, we found [26] enhanced Mo sulfiding degree in unpromoted alumina-supported molybdenum catalysts modified by thioglycolic acid impregnation which addition resulted in partial Mo^{6+} species reduction to Mo^{5+} (by LMCT complexes formation) previously to materials sulfidation.

However, the positive influence on Mo^{6+} (and Mo^{5+}, in our case) to Mo^{4+} conversion of decreased deposited Mo-support interaction due to carbonaceous deposits from SA decomposition during catalyst activation could not be discarded. In this line, the carbon signal observed at binding energy of 288.1–288.9 eV (referred to C 1s signal at 284.6 eV from adventitious carbon) related to O—C═O (carboxyl or ester) groups from organic additive thermal decomposition [72] was registered corresponding data being expressed as C/Al area ratio (column 7 of Table 3). Incremental amount of carbonaceous deposits (that could play "support-like" role [50]) with SA content in sulfided solids was evidenced. Although the amount of those carbonaceous residua was significantly enhanced in SA(3) (see also Sections 3.3 Thermal analysis and 3.4 Raman spectroscopy) as to those in SA(1) the corresponding C/Al area ratio was not notably increased in accordance with extant larger carbonaceous domains of lower dispersion.

Phosphorus dispersion strongly diminished by SA addition (column 8 of Table 3) suggesting polyphosphates formation [6]. Competition between phosphates and organic moieties for adsorptive sites [15] could be the reason of that fact. Due to strong interaction between phosphate anions and the alumina carrier surface after impregnation phosphomolybdates decomposes into tetrahedral molybdates (MoO_4^{2-}) and phosphate groups [73]. Al_2O_3 surface passivation by organic moieties adsorption could contribute in inhibiting that phenomenon [4] preserving the integrity of original Mo species.

Large graphite-like carbonaceous domains in SA(3) (see section 3.4 Raman spectroscopy) could contribute to enhanced phosphates adsorption. In this line, it has been reported that graphitic carbon could act as effective adsorbent for adsorption/removal of phosphate from aqueous solutions [74]. XPS analysis of sulfided sample prepared at SA/Ni = 2, SA(2) in general showed similar composition results as to those of SA(1).

Regarding Ni species (Table 4) the Ni 2p envelope of various samples (Fig. 7) was decomposed by considering three major contributions [75] namely NiS_x (including Ni_3S_2, Ni_9S_8 or NiS, with binding energy between 853.5 and 854.2 eV), oxidic nickel (binding energy ~856.5–857 eV) and NiMoS phase (binding energy 854.8–856 eV). After catalyst activation (Section 2.3 HDS Reaction Test) segregated sulfided Ni species (not integrated in the "NiMoS" phase) could be present forming a number of different compounds. In this line, among others, Ni_3S_2, Ni_9S_8 and NiS species have been identified after submitting oxidic nickel to sulfiding treatments at similar conditions as to those we used (673 K, under H_2S/H_2 flow) [76]. The binding energy of oxidic nickel signal strongly suggested presence of Ni_2O_3 or $Ni(OH)_2$ [77]. As our formulations were just dried (393 K, Section 2.1 Catalysts Synthesis) presence of NiO species was ruled out considering that high temperature (673 K) calcining could be required for its formation [78].

As the energetic resolution of the XPS used could hardly allow correct decomposition of Ni signals just the mentioned species were considered. In addition to the main photoelectron peaks, our Ni XPS plots (Fig. 7) contain broad "shake-up" satellites where the degree of components overlap in corresponding envelopes was severe as those peaks are superimposed. Thus, the nickel species analysis carried out should be considered semiquantitative [79].

Sulfided NiS_x dispersion increased with SA content in studied solids (column 2, Table 4). Monosaccharides from saccarose hydrolysis could be converted to chelating compounds (carboxylic acids) by oxidation during partial Mo^{6+} reduction through Mo-blue formation. For

Table 3
Surface molybdenum, carbon and phosphorous species over various P-doped NiMo/alumina sulfided catalysts prepared with or without saccharose, as determined by XPS analysis. C/Al represents the areal ratio of C signal at BE = 288.1–288.9 eV, over Al peak.

Sample	Mo^{4+}/Al	Mo^{5+}/Al	Mo^{6+}/Al	Mo_T/Al	Mo^{4+}/Mo_T	C/Al	P/Al
SA(0)	0.049	0.009	0.012	0.071	0.697	0.00	0.0241
SA(1)	0.031	0.0042	0.008	0.043	0.724	0.049	0.0154
SA(2)	0.031	0.0041	0.006	0.042	0.748	0.052	0.0134
SA(3)	0.054	0.007	0.015	0.076	0.704	0.054	0.0750

Mo_T (total surface molybdenum) = $Mo^{4+} + Mo^{5+} + Mo^{6+}$.

Table 4
Nickel surface species of various P-doped NiMo/alumina sulfided catalysts prepared with or without saccharose, as determined by XPS analysis.

Cat.	NiS_x/Al	NiMoS/Al	Ni_{Ox}/Al	Ni_T/Al	Ni_S/Ni_T	PR	$(NiMo)_{slabs}$	$(NiMo)_{slabs/DMo}$
SA(0)	0.001	0.004	0.003	0.008	0.63	48.8	0.076	0.38
SA(1)	0.0027	0.0025	0.002	0.007	0.71	34.1	0.081	0.28
SA(2)	0.0029	0.0021	0.003	0.008	0.62	26.7	0.069	0.21
SA(3)	0.006	0.007	0.003	0.016	0.84	46.3	0.140	0.48

Ni_{Ox}, oxidic nickel; NiS, sulfidic nickel = NiS_x + NiMoS; Ni_T (total surface Ni) = NiS_x + NiMoS + Ni_{Ox}; NiS/NiT = 1-(Ni_{Ox}/Ni_T); PR (promotion rate) = (NiMoS/Ni_T) × 100; $(Ni/Mo)_{slabs}$ = promoter ratio = NiMoS/Mo^{4+}; $(Ni/Mo)_{slabs/DMo}$ = (promoter ratio/D_{Mo}). D_{Mo} from Table 2, as determined by HR-TEM data.

instance, in presence of some oxidizing ions glucose could be transformed to saccharic acid [80] this species being able to effectively chelate Ni^{2+} under pH condtions suitable for weak acid ionization. That effect could probably result in improved nickel species dispersion through interaction of organic Ni complex with the alumina carrier [9]. Also, total nickel dispersion was strongly enhanced in the sample of the highest concentration of organic modifier (column 5, Table 4). Although nickel sulfidability augmented with SA concentration in samples that was not necessarily reflected in increased proportion of NiMoS phase (see SA(1) in column 3 of Table 4) as decreased Mo^{4+} dispersion in that sample precluded mixed species formation due to limited sites to accomodate Ni in edge-decorating positions. Due to that, promotion rate (PR, fraction of Ni engaged in forming NiMoS phase, column 7 of Table 4) actually diminished in sacharide-modified catalysts. However, the absolute amount of that highly active phase ("promoter ratio", column 8 of Table 4) was clearly enhanced in materials prepared with SA. That meant that MoS_2 edges could be effectively promoted in solids prepared with organic additive. Following the way of reasoning of Nicosia and Prins [6], impregnated phosphomolybdates complexated with Ni promoter atoms could be preserved on the passivated alumina surface provided by SA deposition that resulting in augmented more homogeneous NiMoS phases formation. In addition, those mixed phases could mostly belong to Type II sites of enhanced HDS activity due to weakened intearction with the alumina carrier. Similarly to the case of Mo entities (Table 3), the XPS analysis of nickel species of an additional sulfided sample prepared at SA/Ni = 2, SA(2) showed similar composition results as to that from SA(1).

Finally, column 9 of Table 4 show amounts of $NiMo_{slabs}$ phase adjusted by considering Mo^{4+} in MoS_2 edges ($(NiMo)_{slabs/DMo}$, D_{Mo} calculated from HR-TEM data, Table 2). Although that parameter diminisihed over SA(1) and SA(2) it was clearly increased in the sample of the highest SA content.

3.8. Dibenzothiophene hydrodesulfurization (DBT HDS) reaction test

Catalytic activity of various sulfided materials is shown in Table 5. As previously reported [9], SA addition by using a non-aged emerald-green impregnating solution resulted in around 22% increase in activity (k^1 basis) as to that over SA(0). However, the effect of utilizing solutions containing partially reduced Mo^{5+} species (Mo-blue) was significantly more pronounced. HDS capability of tested catalysts increased with SA content getting maximum on SA(1) with 77% higher activity as to that of the sample prepared with no saccharose. Further enhanced amount of organic modifier was not reflected in improved HDS activity. Even more, at the highest concentration studied saccharide addition resulted clearly detrimental.

To compare the effect on HDS activity of other organic modifiers on otherwise similar catalysts additional formulations were prepared by using the one-pot impregnation and alike Ni, Mo and P loading as in SA(1) material prepared with Mo-blue solution (see Section 2.1 Catalyst preparation). Corresponding sulfided formulations were tested in the DBT HDS as already described (see Section 2.3 HDS Reaction test). Under those conditions a material simultaneously impregnated with NiMoP and ethylene glycol (EG, at EG/Ni = 1) non-chelating additive showed 17% increase in activity (on pseudo first order kinetic constant basis) as to the non-modified conventional NiMoP catalyst, alike to that previously found [3]. Also, citric acid (CA, at CA/Ni = 1) chelating additive was utilized the corresponding sulfided solid showing just marginal improvement (~6%) in HDS properties, as compared to the reference material. Although the positive effect of using citric acid as chelator of Ni or Co promoters is well known [28,45,81] it is also true that its influence strongly depends on the preparation stage of the organic acid addition [82]. Under the low pH conditions of one-pot impregnating solutions used (see Section 2.1 Catalyst synthesis) weakly acidic CA could not be deprotonated being then unable to form citrate anions that could adequately complexate Ni promoter species. It is worth emphasizing that our investigation was focused in the application of the readily scalable one-pot preparation methodology that could be easily applied in the catalysts production at commercial level. Then, that method was the one used to compare the effect of various organic additives.

Activity trend was similar when adjusted by either total Mo or Mo^{4+} content in formulations (k^2 and k^3 basis, respectively). However, when Mo^{4+} dispersion over various catalysts was taken into account (Table 2, from Eq. (3)) (k^4 basis) differences in S removal capability among various sulfided catalysts were levelled suggesting that amount of Mo^{4+} sites could be playing very important role in HDS advantage over SA(1) and SA(2). Then, augmented number of sulfided Mo active sites seemed to be partially reponsible for the observed improved activity (on a per mass basis, k^1) of SA-containing materials. Finally, when comparing

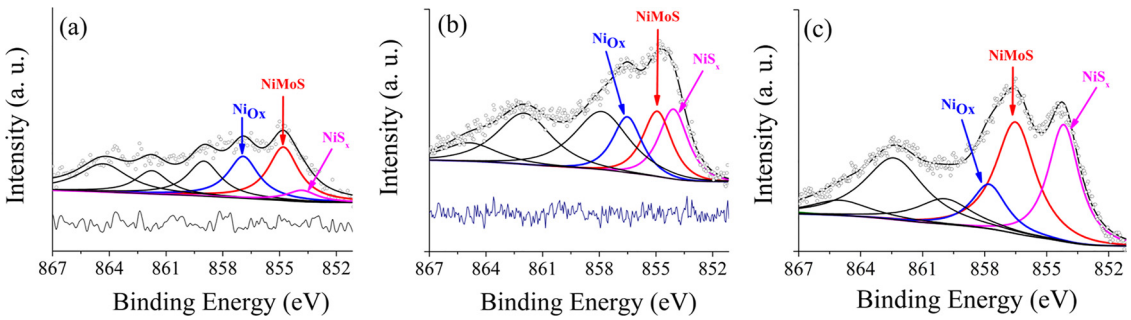

Fig. 7. XPS envelope of Ni $2p_{3/2}$ region of sulfided P-doped NiMo/Al_2O_3 catalysts prepared with or without saccharose. Peak decomposition to various Ni species considered also shown. (a) SA(0); (b) SA(1); (c) SA(3).

Table 5
Pseudo first order kinetic constant values in DBT HDS over sulfided catalysts prepared with and without SA.

Cat.	$k^1 \times 10^{-4}$ $m^3\ kg_{cat}^{-1}\ s^{-1}$	$k^2 \times 10^{-4}$ $l\ g_{Mo}^{-1}\ s^{-1}$	$k^3 \times 10^{-1}$ $l\ mol_{Mo4+}^{-1}\ s^{-1}$	$k^4 \times 10^{-23}$ $at._{Mo4+edge}^{-1}\ s^{-1}$	$k^5 \times 10^{-23}$ $(NiMoS)_{slabs/DMo}^{-1}\ s^{-1}$
SA(0)	1.35	11.25	1.55	1.29	3.38
$SA(1)_g$[a]	1.64	13.71	–	–	–
SA(0.5)	2.04	17.00	–	–	–
SA(1)	2.40	20.04	2.66	1.52	5.43
SA(2)	2.19	18.27	2.34	1.18	5.62
SA(3)	0.28	2.32	0.32	0.18	0.38

k^2 :k^1 adjusted by Mo content in formulations.
k^3:k^2 adjusted by Mo^{4+} content (as determined by XPS analysis, Table 3) in sulfided formulations.
k^4:k^3 adjusted by atomic Mo^{4+} content at edges (as determined by HR-TEM, Table 2) in sulfided formulations.
k^5:Activity per site, k^4 adjusted by $(NiMoS)_{slabs/DMo}$ content (as determined by XPS, Table 4) in sulfided formulations.
[a] Prepared from emerald-green impregnating solution.

HDS performance of various sulfided formulations by adjusting their S removal activity per amount of mixed NiMoS phases entities (k^5 basis, using data from Table 4) on studied catalysts existence of more active sites over materials obtained from Mo-blue precursors seemed to be evidenced. Thus, it appeared that the notably improved DBT conversion registered over SA-modified materials could be provoked by improved dispersion of more active well-promoted Mo^{4+} sites. The former effect originated in shorter MoS_2 slabs of slightly higher stacking (Table 2) whereas support-like [50] carbonaceous residua decreasing deposited species-carrier interaction could result in Type II sites of enhanced HDS intrinsic activity [83]. In this line, formation of Type I structures characterized by existence of Mo—O—Al linkages in the MoS_2 basal plane in direct contact with the carrier surface could be precluded by using weakly interacting supports as carbon [84]. It is worth mentioning that even for the material prepared with no SA the possibility of formation of those Mo—O—Al linkages could be rather low considering that the formulation was non-calcined (just dried at 393 K, see Section 2.1 Catalysts Synthesis). In that case, the amount of Mo species in high interaction with the alumina carrier could be diminished.

Very recently other groups [85] have addressed on the convenienence of existence of carbon overlayers on HDT catalyst supports prior to impregnation of active phases precursors. For instance, glucose has been used as carbon precursor being pore-filling impregnated at various contents over titania carrier where the resulting solids were further annealed at 773 K. Increased activity in DBT HDS was found over corresponding C-containing NiMo sulfided catalysts, that effect being however function of the carbonaceous deposits amount. In that case, the highest activity was registed for materials with around 1–2% of initial carbon whereas the catalytic properties progressively decreased by augmenting C-content in studied solids.

We also found dramatically decreased HDS activity over our SA(3) sample, in spite of containing the highest amount of $(NiMo)_{slabs}$ phase (column 8 of Table 4) among prepared formulations. We consider that the massive amount of carbonaceous deposits over that formulation (see Section 3.4 Raman spectroscopy of impregnated samples) could be playing decisive role on the observed behavior. Also, the strongly diminished porosity (Fig. S5) of the material prepared at the highest SA content could provoke severely hindered accesibility of reactant molecules to active sites. Even more, the corresponding N_2 adsorption isotherm (Fig. S4) strongly suggested formation of inkle-bottle-shaped pores that could significantly affect diffusion/counterdifussion of reactants/products into the catalysts porous network. Additionally, we could not discard the possibility that some of NiMoS phase active sites could be detected although being covered by carbon overlayers considering that XPS probe radiation could penetrate nanometric depths. Then, thus sites could be accounted for but not being available to adsorb reactant molecules. In previous reports, we have observed that on NiMo sulfided catalysts prepared at high organic additive (chitosan) content [86] where large amount of carbon overlayers impeded adsorption of CO probe molecule used during corresponding FTIR studies of corresponding alumina-supported sulfided phases.

Regarding selectivity to various products, DBT conversion could be carried out through direct desulfurization (DDS, to biphenyl) and hydrogenation (HYD, firstly to hydrodibenzothiophenes, HDBT's) [87] reaction pathways, Scheme S2. At our reaction conditions (see Section 2.3 HDS Reaction Test), neither hydroDBT's nor the product from complete saturation of aromatic rings (bicyclohexyl) were observed. Taking into account that BP hydrogenation to cyclohexylbenzene (CHB) could be strongly inhibited by DBT competitive adsorption under our HDS conditions [88], all CHB produced must have predominantly come from HYD route, through rapid sulfur removal of partially saturated HDBT's [88].

No important differences in selectivity in the DBT HDS (at 50% conversion) over various tested sulfided formulations were found (Fig. S10) suggesting similar reaction mechanism over active sites existent over various prepared materials. That fact suggested alike MoS_2 promotion degree by nickel, as it is know that non-efficient molydenum sulfide slab edges decoration by Ni could provoke both diminished HDS activity and decreased selectivity to the product from DDS route (biphenyl) [89]. It has been claimed that when taking place on Type II sites HDS had enhanced selectivity to products from HYD route. However, that seems to be much more evident in catalysts of high Mo loading (~24%) [90]. On the other hand, those authors [90] found that selectivity to species from both reaction pathways (DDS and HYD, DBT HDS) was similar over Type I and Type II catalysts in materials of molybdenum concentration alike as to that used in the present work (14 vs. 12%, respectively)

Sacharose as additive seemed to play several roles that could contribute as a whole in obtaining materials of enhanced sulfur removal activity. However, further studies focused in several aspects that deserve deeper insigth are clearly needed. Among them, specific studies on the exact nature of LMCT complex formed during Mo partial reduction and the identification of possible formation of oxidized by-products (carboxylic acids) that could in turn complexate Ni promoter species should be endeavored.

Through its interesting chemistry saccharose results a highly soluble, cheap and environmentally-friendly non-toxic additive to produce catalysts of enhanced HDS activity.

4. Conclusions

Saccharose (SA) was used as organic additive in simultaneously impregnated P-doped $NiMo/Al_2O_3$ hydrodesulfurization catalyst. Originally emerald-green one-pot impregnating solutions prepared by MoO_3 digestion (~353 K) in diluted aqueous H_3PO_4 followed by nickel hydroxycarbonate addition changed to cobalt-blue by dissolving saccharose (SA, at SA/Ni = 0.5–3) and room-temperature aging (2–4 days, depending on disaccharide concentration). Molybdenum-blue species

characterized by presence of partially reduced Mo^{6+} to Mo^{5+} were evidenced by UV–vis spectroscopy. The originally non-reducing sugar was hydrolyzed under the very acidic conditions (pH ~ 2) of impregnating NiMoP solutions producing fructose and glucose which partially reduced Mo^{6+} to Mo^{5+} species. Monosaccharides oxidation could result in organic acids that could effectively complexate Ni promoter. After sulfiding of nickel-promoted Mo-blue precursors shorter MoS_2 slabs length of enhanced stacking were observed (by HR-TEM). Mo and Ni sulfidability and nickel dispersion (as determined by XPS) increased with the amount of organic modifier. Enhanced hydrodesulfurization activity in liquid-phase dibenzothiophene HDS was registered for catalyst obtained from Mo-blue precursors as to that of corresponding material from conventional emerald-green impregnating solutions (with or without SA). It appeared that carbonaceous deposits from saccharides residua also contributed to enhanced activity through formation of more active sites (Type II) by weakening deposited species-carrier interaction However, in solids impregnated at high saccharose content (SA/Ni = 3) enhanced mixed "NiMoS" phase formation was not reflected in improved activity probably because excessive amount of carbonaceous deposits from SA residua decomposition during catalyst activation partially plugged the porous network (as determined by N_2 physisorption) in sulfided formulations. That fact seemed to provoke limited accessibility of reactant molecules to surface active sites.

Mo-blue precursor obtained through monosaccharides partial reduction seemed to play decisive role in obtaining HDS catalysts of improved properties. Saccharose results a highly soluble, cheap and environmentally-friendly additive to produce catalysts of enhanced HDS activity.

Acknowledgements

The authors acknowledge support through 117086 SENER-CONACYT-Hidrocarburos grant and Y.00105 Project from IMP. A.W. Gutiérrez thanks CONACYT for graduate student scholarship. We also acknowledge to anonymous reviewers whose critical comments and remarks strongly contributed in improving the quality of this manuscript.

Appendix A. Supplementary data

Supplementary material related to this article can be found, in the online version, at doi:https://doi.org/10.1016/j.apcatb.2018.06.034.

References

[1] M.A. Lélias, P.J. Kooyman, L. Mariey, L. Oliviero, A. Travert, J. van Gestel, J.A.R. van Veen, F. Maugé, Effect of NTA addition on the structure and activity of the active phase of cobalt-molybdenum sulfide hydrotreating catalysts, J. Catal. 267 (2009) 14–23.

[2] L. van Haandel, G.M. Bremmer, E.J.M. Hensen, Th. Weber, The effect of organic additives and phosphoric acid on sulfidation and activity of (Co)Mo/Al_2O_3 hydrodesulfurization catalysts, J. Catal. 351 (2017) 95–106.

[3] J. Escobar, M.C. Barrera, J.A. Toledo, M.A. Cortés-Jácome, C. Angeles-Chávez, S. Núñez, V. Santes, E. Gómez, L. Díaz, E. Romero, J.G. Pacheco, Effect of ethyleneglycol addition on the properties of P-doped NiMo/Al_2O_3 HDS catalysts: part I. Materials preparation and characterization, Appl. Catal. B-Environ. 88 (2009) 564–575.

[4] D. Nicosia, R. Prins, The effect of glycol on phosphate-doped CoMo/Al_2O_3 hydrotreating catalysts, J. Catal. 229 (2005) 424–438.

[5] D. Nicosia, R. Prins, The effect of phosphate and glycol on the sulfidation mechanism of CoMo/Al_2O_3 hydrotreating catalysts: an in situ QEXAFS study, J. Catal. 231 (2005) 259–268.

[6] D. Nicosia, R. Prins, ^{31}P MAS NMR and Raman study of a Co(Zn)MoP/γ-Al_2O_3 HDS catalyst precursor containing triethyleneglycol, J. Catal. 234 (2005) 414–420.

[7] P. Mazoyer, C. Geantet, F. Diehl, C. Pichon, T.S. Nguyen, M. Lacroix, In situ EXAFS study of the sulfidation of a hydrotreating catalyst doped with a non chelating organic additive, Oil Gas Sci. Tech. Rev. IFP 60 (2005) 791–799.

[8] V. Costa, K. Marchand, M. Digne, C. Geantet, New insights into the role of glycol-based additives in the improvement of hydrotreatment catalyst performances, Catal. Today 130 (2008) 69–74.

[9] J. Escobar, A. Gutiérrez, M.C. Barrera, J.A. Colín, NiMo/alumina hydrodesulphurization catalyst modified by saccharose: effect of addition stage of organic modifier, Can. J. Chem. Eng. 94 (2016) 66–74.

[10] L. Catita, A.-A. Quoineaud, D. Espinat, C. Pichon, O. Delpoux, Application of magnetic resonance imaging and raman imaging to study the impact of phosphorus in impregnation of hydrotreatment catalysts, Appl. Catal. A-Gen. 547 (2017) 164–175.

[11] A. Pimerzin, A. Mozhaev, A. Varakin, K. Maslakov, P. Nikulshin, Comparison of citric acid and glycol effects on the state of active phase species and catalytic properties of CoPMo/Al_2O_3 hydrotreating catalysts, Appl. Catal. B-Environ. 205 (2017) 93–103.

[12] R. Munirathinam, D. Laurenti, G.D. Pirngruber, D. Uzio, Efficient CoMoS catalysts supported on bio-inspired polymer coated alumina for hydrotreating reactions, Chem. Sel. 2 (2017) 2373–2382.

[13] P.A. Chernavskii, A.Y. Khodakov, G.V. Pankina, J.-S. Girardon, E. Quinet, In situ characterization of the genesis of cobalt metal particles in silica-supported Fischer-Tropsch catalysts using Foner magnetic method, Appl. Catal. A-Gen. 306 (2006) 108–119.

[14] Y. Zheng, Y. Zheng, Z. Li, H. Yu, R. Wang, K. Wei, Preparations of C/SiC composites and their use as supports for Ru catalyst in ammonia synthesis, J. Mol. Catal. A-Chem. 301 (2009) 79–83.

[15] K. Singh, S. Mohan, Kinetic studies of the sucrose adsorption onto an alumina interface, Appl. Surf. Sci. 221 (2004) 308–318.

[16] L. Lin, W. Lin, Y.X. Zhu, B.Y. Zhao, Y.C. Xie, Uniformly carbon-covered alumina and its surface characteristics, Langmuir 21 (2005) 5040–5046.

[17] T. Fujikawa, O. Chiyoda, M. Tsukagoshi, K. Idei, S. Takehara, Development of a high activity HDS catalyst for diesel fuel: from basic research to commercial experience, Catal. Today 45 (1998) 307–312.

[18] L. Kaluža, M. Zdražil, Preparation of bimetallic CoO-MoO_3/γ-Al_2O_3 and NiOMoO_3/γ-Al_2O_3 hydrodesulfurization catalysts by deposition of Co, Ni and Mo onto α-AlOOH during paste processing, React. Kinet. Catal. Lett. 91 (2007) 249–255.

[19] L. Kaluža, M. Zdražil, Z. Vít, Deposition of NiO onto MoO_3/γ-Al_2O_3 extrudates by slurry impregnation method, React. Kinet. Catal. Lett. 97 (2009) 307–313.

[20] M. Dorneles de Mello, F. de Almeida Braggio, B. da Costa Magalhães, J.L. Zotin, M. Antunes Pereira da Silva, Effects of phosphorus content on simultaneous ultradeep HDS and HDN reactions over NiMoP/alumina catalysts, Ind. Eng. Chem. Res. 56 (37) (2017) 10287–10299.

[21] J. Escobar, J.A. Toledo, A.W. Gutiérrez, M.C. Barrera, M.A. Cortés, C. Angeles, L. Díaz, Stud. Surf. Sci. Catal. 175 (2010) 767–770.

[22] X. Wang, P. Du, K. Chi, A. Duan, Ch. Xu, Zh. Zhao, Zh. Chen, H. Zhang, Synthesis of NiMo catalysts supported on mesoporous silica FDU-12 with different morphologies and their catalytic performance of DBT HDS, Catal. Today 291 (2017) 146–152.

[23] P. Blanchard, E. Payen, J. Grimblot, L. Le Bihan, O. Poulet, R. Loutaty, J. Mol. Catal. A-Chem. 135 (1998) 143–153.

[24] S. Kasztelan, H. Toulhoat, J. Grimblot, J.P. Bonnelle, A geometrical model of the active phase of hydrotreating catalysts, Appl. Catal. 13 (1984) 127–159.

[25] X. Xu, P. Waller, E. Crezee, Z. Shan, F. Kapteijn, J.A. Moulijn, Preparation of mesoporous highly dispersed Pd-Pt catalysts for deep hydrodesulfurization, Stud. Surf. Sci. Catal. 143 (2002) 1019–1026.

[26] J.A. Toledo-Antonio, M.A. Cortés-Jácome, J. Escobar-Aguilar, C. Angeles-Chavez, J. Navarrete-Bolaños, E. López-Salinas, Upgrading HDS activity of MoS_2 by thioglycolic acid complex with MoOx supported on the alumina, Appl. Catal. B-Environ. 213 (2017) 106–117.

[27] K. Hadjiivanov, M. Mihaylov, D. Klissurski, P. Stefanov, N. Abadjieva, E. Vassileva, L. Mintchev, Characterization of Ni/SiO_2 catalysts prepared by successive deposition and reduction of Ni^{2+} ions, J. Catal. 185 (1999) 314–323.

[28] V.A. Suárez-Toriello, C.E. Santolalla-Vargas, J.A. de los Reyes, A. Vázquez-Zavala, M. Vrinat, C. Geantet, Influence of the solution pH in impregnation with citric acid and activity of Ni/W/Al_2O_3 catalysts, J. Mol. Catal. A-Chem. 404 (2015) 36–46.

[29] P.J. Charley, B. Sarkar, C.F. Stitt, P. Saltman, Chelation of iron by sugars, Biochim. Biophys. Acta 69 (1963) 313–321.

[30] P.S. Davis, D.J. Deller, Prediction and demonstration of iron chelating ability of sugars, Nature 212 (1966) 404–405.

[31] M.Y. Shukor, M.F. Rahman, Z. Suhaili, N.A. Shamaan, M.A. Syed, Hexavalent molybdenum reduction to Mo-blue by acinetobacter calcoaceticus, Folia Microbiol. 55 (2) (2010) 137–143.

[32] K. Yoshimura, M. Ishii, T. Tarutani, Micro-determination of phosphate in water by gel-phase colorimetry with Mo-blue, Anal. Chem. 58 (1986) 591–594.

[33] C.V. Cáceres, J.L.G. Fierro, J. Lázaro, A. López Agudo, J. Soria, Effect of support on the surface characteristics of supported molybdena catalysts, J. Catal. 122 (1990) 113–125.

[34] C. Louis, M. Che, EPR and diffuse reflectance studies of the physico-chemical phenomena occurring during the preparation of Mo/SiO_2 catalysts by the grafting method, J. Catal. 135 (1992) 156–172.

[35] X. Liu, M. Conte, W. Weng, Q. He, R.L. Jenkins, M. Watanabe, D.J. Morgan, D.W. Knight, D.M. Murphy, K. Whiston, C.J. Kiely, G.J. Hutchings, Molybdenum blue nano-rings: an effective catalyst for the partial oxidation of cyclohexane, Catal. Sci. Technol. 5 (2015) 217–227.

[36] D.C. LaMont, A.J. Gilligan, A.R.S. Darujati, A.S. Chellappa, W.J. Thomson, The effect of Mo_2C synthesis and pretreatment on catalytic stability in oxidative reforming environments, Appl. Catal. A-Gen. 255 (2003) 239–253.

[37] Z. Vít, D. Gulková, M. Novák, Preparation of alumina supported Mo catalysts from molybdenum blue precursor, React. Kinet. Catal. Lett. 55 (1995) 221–226.

[38] R. Srinivasan, H.C. Liu, S.W. Weller, Sintering of "shell" molybdena-alumina catalysts, J. Catal. 57 (1979) 87–95.

[39] T.J. Han, An improved phosphorus assay for oils without carcinogenic hydrazine sulfate, JAOCS 72 (8) (1995) 881–885.

[40] K.-H. Tytko, Mo supplement volumen B 3b molybdate ions, in: H. Katscher,

F. Shröoder (Eds.), Gmelin Handbook of Inorganic Chemistry, 8th ed., Springer-Verlag, Berlin, Heidelberg GmbH, 1989pp. 15–16.
[41] L. Xu, B. Wei, Zh Zhang, Zh Lü, H. Gao, Y. Zhang, Synthesis and luminescence of europium doped yttria nanophosphors via a sucrose-templated combustion method, Nanotechnology 17 (2006) 4327–4331.
[42] S.G. Leofanti, M. Padovan, G. Tozzola, B. Venturelli, Surface area and pore texture of catalysts, Catal. Today 41 (1998) 207–219.
[43] W. Zhou, M. Liu, Q. Zhang, Q. Wei, S. Ding, Y. Zhou, Synthesis of NiMo catalysts supported on gallium containing mesoporous Y zeolites with different gallium contents and their high activities in the hydrodesulfurization of 4,6-dimethyldibenzothiophene, ACS Catal. 7 (11) (2017) 7665–7679.
[44] S.P. Rigby, R.S. Fletcher, Experimental evidence for Pore blocking as the mechanism for nitrogen sorption hysteresis in a mesoporous material, J. Phys. Chem. B 108 (2004) 4690–4695.
[45] N. Rinaldi, T. Kubota, Y. Okamoto, Effect of citric acid addition on Co-Mo/B_2O_3/Al_2O_3 catalysts prepared by a post-treatment method, Ind. Eng. Chem. Res. 1090 (2009) 10414–10424.
[46] J.C. Groen, L.A.A. Peffer, J. Pérez-Ramírez, Pore size determination in modified micro- and mesoporous materials. Pitfalls and limitations in gas adsorption data analysis, Microporous Mesoporous Mater. 60 (2003) 1–17.
[47] Y. Wang, L. Lin, B.S. Zhu, Y.X. Zhu, Y.C. Xie, Different dispersion behavior of glucose and sucrose on alumina and silica surfaces, Appl. Surf. Sci. 254 (2008) 6560–6567.
[48] M. Kosmulski, The pH-dependent surface charging and points of zero charge: v. Update, J. Colloid Interface Sci. 353 (2011) 1–15.
[49] S. Braun, L.G. Appel, M. Schmal, Molybdenum species on alumina and silica supports for soot combustion, Catal. Commun. 6 (2005) 7–12.
[50] H. Ge, X.-D. Wen, M.A. Ramos, R.R. Chianelli, Sh. Wang, J. Wang, Zh. Qin, Zh. Lyu, X. Li, Carbonization of ethylenediamine Co-impregnated CoMo/Al_2O_3 catalysts sulfided by organic sulfiding agent, ACS Catal. 4 (8) (2014) 2556–2565.
[51] R. Palcheva, L. Kaluža, L. Dimitrov, G. Tyuliev, G. Avdeev, K. Jirátová, A. Spojakina, NiMo catalysts supported on the Nb modified mesoporous SBA-15 and HMS: effect of thioglycolic acid addition on HDS, Appl. Catal. A-Gen. 520 (2016) 24–34.
[52] J.A. Bergwerff, T. Visser, B.R.G. Leliveld, B.D. Rossenaar, K.P. de Jong, B.M. Weckhuysen, Envisaging the physicochemical processes during the preparation of supported catalysts: raman microscopy on the impregnation of Mo onto Al_2O_3 extrudates, J. Am. Chem. Soc. 126 (2004) 14548–14556.
[53] H. Kraus, R. Prins, Composition of impregnation solutions and wet impregnated Mo-P/γ -Al_2O_3 catalysts as investigated by ^{31}P and ^{95}Mo NMR, J. Catal. 164 (1996) 251–259.
[54] J. Chen, J. Mi, K. Li, X. Wang, E. Dominguez Garcia, Y. Cao, L. Jiang, L. Oliviero, F. Mauge, The role of citric acid in preparing highly active CoMo/Al_2O_3 catalyst: from aqueous impregnation solution to active site formation, Ind. Eng. Chem. Res. 56 (48) (2017) 14172–14181.
[55] Y. Okamoto, T. Imanaka, Interaction chemistry between molybdena and alumina: infrared studies of surface hydroxyl groups and adsorbed carbon dioxide on aluminas modified with molybdate, sulfate, or fluorine anions, J. Phys. Chem. 92 (1988) 7102–7112.
[56] A.N. Desikan, L. Huang, S.T. Oyama, Structure and dispersion of molybdenum oxide supported on alumina and titania, J. Chem. Soc. Faraday Trans. 88 (22) (1992) 3357–3365.
[57] T.L. Drake, P.C. Stair, Multiwavelength Raman spectroscopic characterization of alumina-supported molybdenum oxide prepared by vapor deposition, Top. Catal. 60 (19–20) (2017) 1618–1630.
[58] Á. Ibarra, A. Veloso, J. Bilbao, J.M. Arandes, P. Castaño, Dual coke deactivation pathways during the catalytic cracking of raw bio-oil and vacuum gasoil in FCC conditions, Appl. Catal. B-Environ. 182 (2016) 336–346.
[59] N.R. Arutyunyan, M.S. Komlenok, E.V. Zavedeev, S.M. Pimenov, Raman spectroscopy of amorphous carbon films modified by single-pulse irradiation of nanosecond and femtosecond lasers, Phys. Status Solidi B 255 (1–6) (2018) 1700225.
[60] N.M. Rodriguez, R.T.K. Baker, Interaction of hydrogen with metal sulfide catalysts. Direct observation of spillover, J. Catal. 140 (1993) 287–301.
[61] P.A. Nikulshin, N.N. Tomina, A.A. Pimerzin, A.V. Kucherov, V.M. Kogan, Investigation into the effect of the intermediate carbon carrier on the catalytic activity of the HDS catalysts prepared using heteropolycompounds, Catal. Today 149 (2010) 82–90.
[62] W. Zhong, M. Liu, J. Dai, J. Yang, L. Mao, D. Yin, Synergistic hollow CoMo oxide dual catalysis for tandem oxygen transfer: preferred aerobic epoxidation of cyclohexene to 1,2-epoxycyclohexane, Appl. Catal. B-Environ. 225 (2018) 180–196.
[63] J. Ramírez, R. Contreras, P. Castillo, T. Klimova, R. Zárate, R. Luna, Characterization and catalytic activity of CoMo HDS catalysts supported on alumina-MCM-41, Appl. Catal. Gen. 197 (2000) 69–78.
[64] X. Wang, Zh. Zhao, P. Zheng, Zh. Chen, A. Duan, Ch. Xu, J. Jiao, H. Zhang, Zh. Cao, B. Ge, Synthesis of NiMo catalysts supported on mesoporous Al_2O_3 with different crystal forms and superior catalytic performance for the hydrodesulfurization of dibenzothiophene and 4,6-dimethyldibenzothiophene, J. Catal. 344 (2016) 680–691.
[65] S. Eijsbouts, On the flexibility of the active phase in hydrotreating catalysts, Appl. Catal. A-Gen. 158 (1997) 53–92.
[66] P.A. Nikulshin, A.V. Mozhaev, A.A. Pimerzin, V.V. Konovalov, A.A. Pimerzin, CoMo/Al_2O_3 catalysts prepared on the basis of Co_2Mo_{10}-heteropolyacid and cobalt citrate: effect of Co/Mo ratio, Fuel 100 (2012) 24–33.
[67] H. Topsøe, The role of Co–Mo–S type structures in hydrotreating catalysts, Appl. Catal. A-Gen. 322 (2007) 3–8.
[68] X. Yi, D. Guo, P. Li, X. Lian, Y. Xu, Y. Dong, W. Lai, W. Fang, One pot synthesis of NiMo-Al_2O_3 catalysts by solvent-free solid-state method for hydrodesulfurization, RSC Adv. 7 (2017) 54468–54474.
[69] P. Beccat, P. Da Silva, Y. Huiban, S. Kasztelan, Quantitative surface analysis by XPS (X-ray photoelectron spectroscopy): application to hydrotreating catalysts, Oil Gas Sci. Technol. Rev. IFP 54 (1999) 487–496.
[70] F. Pagnanelli, F. Ferella, I. De Michelis, F. Vegliò, Adsorption onto activated carbon for molybdenum recovery from leach liquors of exhausted hydrotreating catalysts, Hydrometallurgy 110 (2011) 67–72.
[71] Y. Nath Prajapati, N. Verma, Hydrodesulfurization of thiophene on activated carbon fiber-supported NiMo catalysts, Energy Fuels 32 (2) (2018) 2183–2196.
[72] N. Frizi, P. Blanchard, E. Payen, P. Baranek, C. Lancelot, M. Rebeilleau, C. Dupuy, J.P. Dath, Genesis of new gas oil HDS catalysts: study of their liquid phase sulfidation, Catal. Today 130 (2008) 32–40.
[73] W.-C. Chenh, N.P. Luthra, NMR study of the adsorption of phosphomolybdates on alumina, J. Catal. 109 (1988) 163–169.
[74] S. Vasudevan, J. Lakshmi, The adsorption of phosphate by graphene from aqueous solution, RSC Adv. 2 (2012) 5234–5242.
[75] B. Guichard, M. Roy-Auberger, E. Devers, C. Legens, P. Raybaud, Aging of Co(Ni)MoP/Al_2O_3 catalysts in working state, Catal. Today 130 (2008) 97–108.
[76] A. Olivas, J. Cruz-Reyes, V. Petranovskii, M. Avalos, S. Fuentes, J. Vac. Sci. Technol. A 16 (1998) 3515–3520.
[77] B.W. Hoffer, A.D. van Langeveld, J.-P. Janssens, R.L.C. Bonné, C.M. Lok, J.A. Moulijn, Stability of highly dispersed Ni/Al_2O_3 catalysts: effects of pretreatment, J. Catal. 192 (2000) 432–440.
[78] N.N.M. Zorkiplia, N.H.M. Kausb, A.A. Mohamada, Synthesis of NiO nanoparticles through sol–gel method, Procedia Chem. 19 (2016) 626–631.
[79] J. Stoch, A. Capecki, Decomposition of $2p_{3/2}$ bands in XPS spectra of Fe, Co and Ni compounds, Surf. Interface Anal. 15 (1990) 206–210.
[80] J.-S. Girardon, E. Quinet, A. Griboval-Constant, P.A. Chernavskii, L. Gengembre, A.Y. Khodakov, Cobalt dispersion, reducibility, and surface sites in promoted silica-supported Fischer–Tropsch catalysts, J. Catal. 248 (2007) 143–157.
[81] S.L. González-Cortés, Y. Qian, H.A. Almegren, T. Xiao, V.L. Kuznetsov, P.P. Edwards, Citric acid-assisted synthesis of γ-alumina-supported high loading CoMo sulfide catalysts for the hydrodesulfurization (HDS) and hydrodenitrogenation (HDN) reactions, Appl. Petrochem. Res. 5 (2015) 181–197.
[82] J. Escobar, M.C. Barrera, A.W. Gutiérrez, J.E. Terrazas, Benzothiophene hydrodesulfurization over NiMo/alumina catalysts modified by citric acid. Effect of addition stage of organic modifier, Fuel Process. Technol. 156 (2017) 33–42.
[83] R. Candia, J. Villadsen, N.-Y. Topsøe, B.S. Clausen, H. Topsøe, Active phase in sulfided NiMo/γ-Al_2O_3 catalyst, Bull. Soc. Chim. Belg. 93 (1984) 763–773.
[84] F. Besenbacher, M. Brorson, B.S. Clausen, S. Helveg, B. Hinnemann, J. Kibsgaard, J.V. Lauritsen, P.G. Moses, J.K. Nørskov, H. Topsøe, S.T.M. Recent, DFT and HAADF-STEM studies of sulfide-based hydrotreating catalysts: insight into mechanistic, structural and particle size effects, Catal. Today 130 (2008) 86–96.
[85] L. Li, H. Yue, Sh. Chen, L. Huang, X. Li, Zh. Yang, X. Lu, Interfacial engineering of NiMo/Mesoporous TiO_2 catalyst with carbon for enhanced hydrodesulfurization performance, Catal. Lett. 148 (3) (2018) 992–1002, http://dx.doi.org/10.1007/s10562-018-2308-5.
[86] G. Ríos-Caloch, V. Santes, J. Escobar, M. Valle-Orta, M.C. Barrera, M. Hernández-Barrera, Effect of chitosan addition on NiMo/Al_2O_3 catalysts for dibenzothiophene hydrodesulfurization, Int. J. Chem. React. Eng. 10 (1) (2012) 1–24. A71.
[87] M. Houalla, N.K. Nag, A.V. Sapre, D.H. Broderick, B.C. Gates, Hydrodesulfurization of dibenzothiophene catalyzed by sulfided CoO-MoO_3/γ-Al_2O_3: the reaction network, AIChE J. 24 (1978) 1015–1021.
[88] E.J.M. Hensen, P.J. Kooyman, Y. van der Meer, A.M. van der Kraan, V.H.J. de Beer, J.A.R. van Veen, R.A. van Santen, The relation between morphology and hydrotreating activity for supported MoS_2 particles, J. Catal. 199 (2) (2001) 224–235.
[89] F. Bataille, J.L. Lemberton, P. Michaud, G. Pérot, M. Vrinat, M. Lemaire, E. Schulz, M. Breysse, S. Kasztelan, Alkyldibenzothiophenes hydrodesulfurization-promoter effect, reactivity, and reaction mechanism, J. Catal. 191 (2000) 409–422.
[90] N. Kagami, B.M. Vogelaar, A.D. van Langeveld, J.A. Moulijn, Reaction pathways on NiMo/Al_2O_3 catalysts for hydrodesulfurization of diesel fuel, Appl. Catal. A-Gen. 293 (2005) 11–23.